The optical design of FLITECAM

J. M. M. Horn and I. S. McLean

University of California, Los Angeles, Division of
Astronomy and Astrophysics, 405 Hilgard Avenue, Los Angeles, CA 90095-1562

ABSTRACT

FLITECAM is a facility class instrument on SOFIA, operating from 1-5 microns. A 1024×1024 InSb ALADDIN II array will be used in a fully refractive optics system that provides three optical modes; imaging at a plate scale of $0.47'' \times 0.47''$ per pixel and a field of view of $8'$, grism spectroscopy with moderate resolutions of about R = 1000-2000 depending on the slit width used, and a pupil viewing mode. The plate scale is achieved by using an f/4.8 back-end camera behind an f/4.9 collimator. The $8'$ field of view of SOFIA's f/19.6 telescope translates to a focal plane aperture of 114 mm. The collimator optics are therefore quite large with a diameter of almost 170 mm. Between the pupil image produced by the collimator and the f/4.8 camera, a set of three lenses will be inserted to achieve a pupil viewing mode. The optical train is entirely refractive, with triplets or split triplets using combinations of LiF, BaF_2, ZnS and ZnSe. The design of an optics system with this wide a wavelength range of more than two octaves and the large field of view present a challenging project. We demonstrate that our optical design meets the performance requirements with certain allowed lens-fabrication and misalignments built in.

Keywords: SOFIA, infrared, imaging, grism, spectroscopy, optics

1. INTRODUCTION

FLITECAM is the First Light Infrared Test Experiment Camera on SOFIA* with the main purpose of testing the SOFIA telescope assembly in the near infrared wavelength region from 1-5 microns.[1] SOFIA has a 2.5 m bent Cassegrain f/19.6 telescope on a Boeing 747SP. Its operating altitudes will be about 41,000 ft. SOFIA will therefore fly above 99 % of the atmosphere's water content, leaving about 5 μm - 10 μm water column above it. The mid infrared region from about 30 to 300 microns, which is opaque from the ground, therefore becomes about 80 % transparent, with some water absorption lines and almost spaceborne conditions between them. From 4 μm to 600 μm atmospheric transmission is still significant better than from the ground.[2]

FLTIECAM was originally planned with a 512×512 array, a plate scale of $0.47''$ per pixel and a $4' \times 4'$ field of view. Recently it has been upgraded to 1024×1024 with the same plate scale but an $8'$ field of view in response to a recommendation by the review board of the preliminary design review. This upgrade path will allow FLITECAM to be very efficient not only in the test period. This is because the entire SOFIA field of $8'$ diameter has to be tested, so that various tests can be done with just one flight. But also for science applications, this field of view is very valuable.[3] In order to partly compensate for the higher cost involved in the overall larger optics, a high-resolution imaging mode with a plate scale of $0.12''$ has been taken out of the system. This would have been useful to resolve the seeing limited PSF, rather than for science purposes, and was therefore only a goal. However, the possibility on implementing a warm scale changer to match that plate scale in front of FLITECAM in the first year of operation is under investigation.

FLITECAM's function as a test camera for a newly built telescope imposes another important requirement on the instrument. It has to be fully checked out before it can test the SOFIA telescope. For this purpose, it is planned to deploy FLITECAM on at least one ground-based telescope well before the SOFIA telescope test period. This will happen at Lowell Observatory's 72-inch Perkins telescope in Flagstaff, AZ. Because FLITECAM will be operating jointly with the High-speed Occultation Photometer/Imager (HOPI) for SOFIA test purposes as well as for

Further author information: (Send correspondence to J. M. M. Horn)
J. M. M. Horn: E-mail: horn@astro.ucla.edu, www: http://flitecam.astro.ucla.edu
*Stratospheric Observatory for Infrared Astronomy

occultation measurements, this is the dedicated telescope for a thorough test run. It is planned to install FLITECAM on a regular basis at the 3-meter Shane telescope at Lick Observatory on Mt. Hamilton, CA. Even after the SOFIA test period, FLITECAM will be a valuable infrared instrument at Lick given its plate scale, that matches local seeing very well, and the large field of view.

In this paper, we will discuss FLITECAM's optics design, which is frozen at this point of the project. Testplates for all lens surfaces have been found from Optical Solutions Inc. (OSI) as well as from Janos Inc. The final vendor has not yet been chosen, and because both designs show virtually the same performance, we picked the OSI setup to demonstrate the performance results. In the next section we first give a brief overview of the system design before we discuss the requirements imposed on the optical design considerations. Then we present the actual design, its performance and discuss the tolerance analysis.

2. REQUIREMENTS

The requirements for the optics design are mainly derived from the SOFIA telescope assembly test plan.[1] The details of this test plan which are relevant for the overall FLITECAM camera design are discussed elsewhere.[4,3] Here we summarize the relevant derived requirements for the optics.

- A plate scale of $0.47''$ per pixel is required to critically sample best seeing at $5\,\mu$m
- SOFIA's entire $8'$ circular field of view has to be tested
- The camera needs to be achromatic from 1.0 - 5.0 microns, so that no re-focussing is necessary
- At 5 microns, 80 % of the energy shall fall in one pixel
- The camera throughput should be $\gtrsim 30\,\%$
- There has to be a pupil so that a cold stop, filters, grisms, and other possible optics components, can be inserted
- The pupil size shall be as small as possible in order to keep the cost for filters low
- The re-imaging of the pupil requires at least 256×256 pixels. As we have a 1024×1024 array, this translates to very loose requirements for the pupil re-imager, as we could bin 4 pixels together

Other aberrations like field distortion or lateral color were not specifically mentioned but have to be reasonably low as well.

Other than that, the optics design has to match into an envelope that permits it to be co-mounted with HOPI not only on SOFIA, but also on the Perkins telescope. On Perkins as well as on SOFIA, some mechanical restrictions apply that require FLITECAM to be as small as possible.

3. THE OPTICS DESIGN

Given the list of requirements, a cold pupil has to be generated, which means having a collimator that produces a well defined pupil image in order to insert filters, grisms and to re-image the pupil. In the default imaging mode, a back-end camera has to produce the appropriate plate scale and field of view. After finishing the conceptual study, the optics design has been optimized using commercial optics design software.[5] The SOFIA telescope has been included in the optimization.

3.1. Glass Choice

In the 1-5 micron range, there are not too many suitable glasses one can choose from for a camera design. Standard glasses are low-index fluorides like CaF_2, BaF_2 or LiF and high-index materials like ZnS or ZnSe.

Those five different materials are exclusively in use for FLITECAM, CaF_2 though only for the window. The required wavelength range for the FLITECAM optics spans more than two octaves and simultaneously a large field of view of $8'$ has to be covered. Therefore, doublets for the collimator or back-end camera are unlikely to meet all required specifications. Triplets though should work, and residual aberrations could possibly be reduced by using split triplets or other more complex lens systems.[6,7] Cryogenic index data were available from two different sources[8,9]

and match to within ±0.0002 to ±0.0005. The indices and thermal coefficients of expansion of the materials that are used for FLITECAM have been successfully used previously in other near-infrared instruments.[10] There, triplets using the glass combination BaF_2-LiF-ZnS have been found to provide good performance. Nevertheless, for this work, several other combinations have been studied in order to find out the best one.

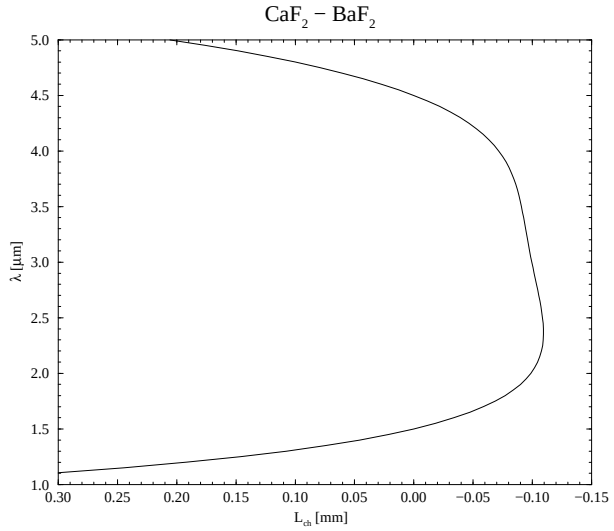

Figure 1. *Secondary Spectrum $L_{ch}(\lambda)$ of a CaF_2-BaF_2 doublet with a nominal focal length of $f_0 = 140\,mm$. The two optimization base points on the wavelength scale were $1.5\,\mu m$ and $4.5\,\mu m$.*

To answer the question what glass combinations are most useful in a doublet or triplet, the secondary and tertiary spectra[11] respectively, have been studied. Secondary spectra for doublets and tertiary spectra for triplets are a measure for their achromatism. The considerations we present are not directly useful for quantitative analysis because they assume thin lenses without center air-spacing. In cryogenic systems each lens must have an air-spacing due to the different thermal expansion coefficients of the various materials in use. And the thin lens approximation is usually violated as well. However, as we will show, it is possible to make qualitative statements on the usefulness of a certain glass combination. Fine tuning of the lens surfaces has then been done with the optics design software, and as predicted, the best glass combinations for the ideal triplets gave good performance outputs in the design simulation see Sect. 3.2.

As expected, not any doublet combination of the above materials met the required achromatism in the secondary spectrum L_{ch}, which is defined by[11]:

$$
\begin{aligned}
L_{ch}(\lambda) &= -\frac{f_0\left(P_c^{(1)}(\lambda) - P_c^{(2)}(\lambda)\right)}{V_d^{(1)}(\lambda) - V_d^{(2)}(\lambda)}, \quad \text{with} \\
V_d^{(i)}(\lambda) &= \frac{n^{(i)}(\lambda - 1)}{n^{(i)}(\lambda_0) - n^{(i)}(\lambda_1)}, \quad \text{and} \\
P_c^{(i)}(\lambda) &= \frac{n^{(i)}(\lambda_0) - n^{(i)}(\lambda)}{n^{(i)}(\lambda_0) - n^{(i)}(\lambda_1)},
\end{aligned}
$$

with f_0 the nominal focal length of the camera, $P_c^{(i)}$ the partial dispersion of the i-th lens material, $V_d^{(i)}$ the Abbe number of the i-th lens material, n the refractive index. λ_0 and λ_1 are two wavelengths for which the secondary spectrum is zero and are typically placed near the lower and upper end of the wavelength range respectively. The best combination turned out to be CaF_2-BaF_2, as shown in Fig. 1 (with $\lambda_0 = 1.5\,\mu m$ and $\lambda_1 = 4.5\,\mu m$), but it still is not acceptable.

For an ideal system of focal length $f = 140\,mm$, the tertiary spectra of several triplets have been evaluated as described by Kingslake.[11] Best results have been found with combinations of BaF_2, LiF and either ZnS or ZnSe,

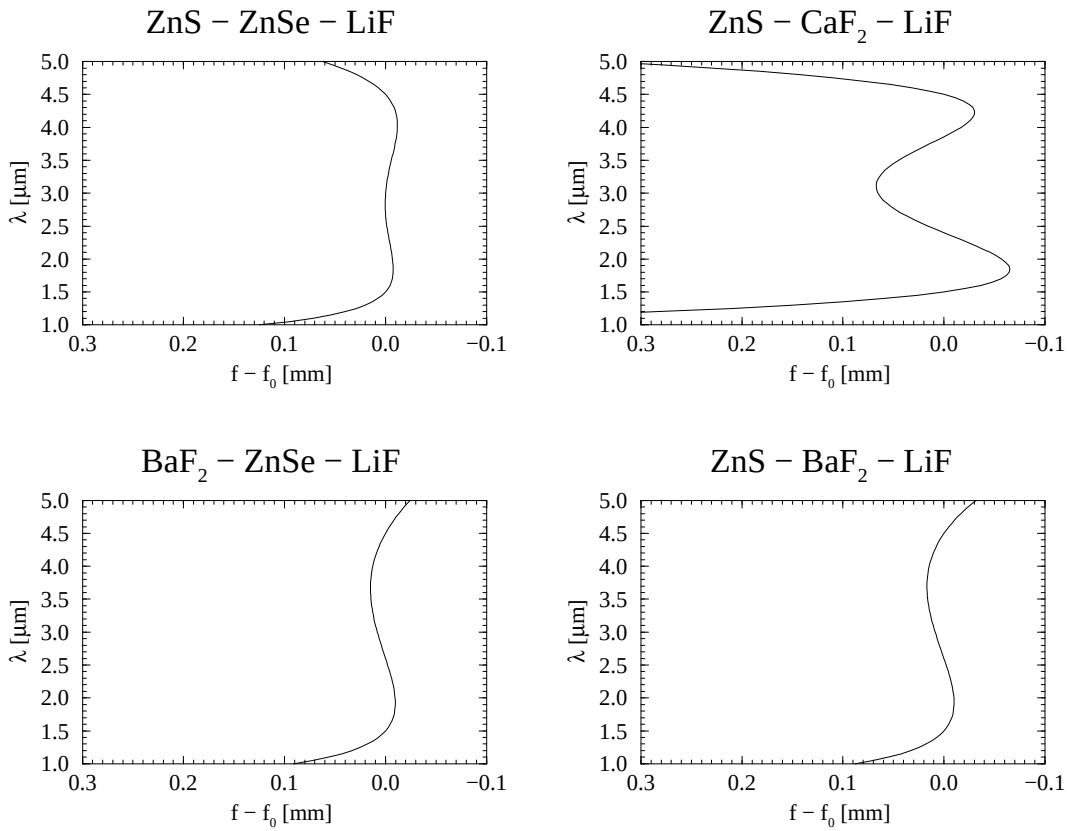

Figure 2. *Tertiary spectra of several different ideal triplets of nominal focal length $f_0 = 140\,mm$, to find the glass combination with the least chromatic aberration possible.*

see Fig. 2. From the analysis of chromatic aberrations alone, no preference in the order of the materials could be found. During the overall optimization process it has been found that ZnS-BaF_2-LiF worked out very good for the collimator triplet, and BaF_2-ZnSe-LiF together with a ZnS-ZnSe doublet got best performance for the split triplet of the f/4.8 back-end camera. Those systems are described in more detail in Sect. 3.2.

3.2. Imaging

3.2.1. The Collimator

Generally, the pupil is desired to be small in order to keep the instrument less complex. In that case, lenses and filters are smaller and less expensive. There is though a trade off, because achieving good optical performance becomes more difficult seeking for smaller pupil sizes with a given wavelength range and field of view, which in case of FLITECAM are quite large. The collimator design needs special emphasis, as it has to accommodate imaging as well as pupil viewing. This is especially true, as we use the back-end camera for both imaging and pupil viewing.

Lens #	Material	Radius front/back [mm]	Center Thickness [mm]	Diameter [mm]
1	ZnS	227.8888 (CX)/191.3560 (CC)	20	168
2	BaF_2	216.3572 (CX)/398.1094 (CX)	35	164
3	LiF	322.7324 (CC)/696.0870 (CX)	21.3	160

Table 1. *The prescription data of the collimator triplet. Not listed are the air-spacings between the lenses, which are 2 mm or more (center air or edge air, whatever is smaller). The high precision in the radii of curvature is a result of conversion from inches to millimeter. (CC = concave, CX = convex)*

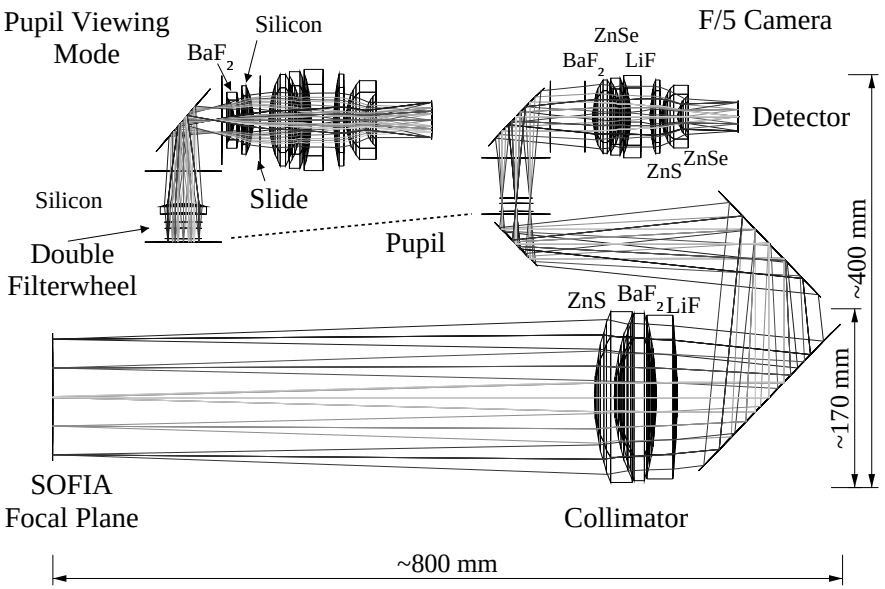

Figure 3. *The FLITECAM optics design. Shown is the default f/4.8 imaging mode and in the upper left corner, the pupil viewing mode. To the lower left is the SOFIA focal plane, and not shown is the CaF_2 window about 2 inches to the left of the focal plane. Four fold mirrors have been implemented to keep the design as compact as possible.*

Lens #	Material	Radius front/back [mm]	Center Thickness [mm]	Diameter [mm]
1	BaF_2	69.92112 (CX)/69.92112 (CX)	25.00	72
2	ZnSe	62.6618 (CC)/89.9922 (CX)	7.20	76
3	LiF	110.7999 (CC)/plano	10.60	80
4	ZnS	139.9540 (CX)/plano	9.00	72
5	ZnSe	45.27296 (CX)/26.29916 (CC)	16.78	62

Table 2. *The prescription data of the f/4.8 split triplet. Not listed are the air-spacings between the lenses, which are 2 mm or more. The high precision in the radii of curvature is a result of conversion from inches to millimeter. (CC = concave, CX = convex)*

For pupil viewing though, we insert another set of lenses between the pupil and the back-end camera to collimate the pupil rays, which are then re-imaged by the back-end camera. So e. g. the parallelism of the rays exiting the collimator plays an important role in finding easy solutions for the imaging back-end camera as well as for the pupil viewing lenses in combination with the back-end camera. For FLITECAM, we found an f/5 collimator triplet to meet all our needs. It produces a pupil of about 28 mm diameter. The $8'$ field of view is equivalent to an aperture size of 114 mm diameter at the telescope focal plane. This dimension and the collimator speed result in a respectable size of about 170 mm diameter of the lenses weighing 5.6 kg all together. The lens combination is ZnS-BaF_2-LiF, and all surfaces are spherical, which is true for all other lenses too. The collimator lens data is shown in Tab. 1.

The $8'$ field of view that FLITECAM has to cover together with the wide wavelength range of 1 - 5 microns prohibits the use of an off-axis parabola as a collimator because the the reflection angle needs to be around 10°, which produces significant aberrations. In the imaging mode, those aberrations could largely be compensated, although the performance was still not as good as for the refractive back-end camera. But no satisfactory solution has been found for the pupil viewing mode, because the pupil image formed by the collimator was too poor.

3.2.2. The Back-end Camera

The first order properties of the back-end camera following the collimator are derived from the SOFIA telescope parameters and the plate scale requirement. The SOFIA f/19.6 telescope assembly, produces a field of $8'$ which is equivalent to 114 mm diameter at the focal plane. With an f/4.8 camera the plate scale of $0.47''$ can therefore

be achieved. Enough space between the pupil image and the re-imaging camera has to be designed in to provide sufficient space to insert a cold stop, filters, and grisms. In another configuration, the pupil has to be re-imaged. It turned out that by providing sufficient space, another set of lenses can be inserted between the pupil formed by the collimator and the f/4.8 lens. In our design, this saved us one mechanism and three lenses. But the space to put in the additional opto-mechanics results in a larger clear aperture of the f/4.8 lenses and therefore in larger aberrations of the meridional rays. The basic lens prescription data are given in Tab. 2, and a picture of the optics design together with the back-end part of the pupil viewing mode is shown in Fig. 3.

In Fig. 4, some representative results of the performance in the imaging mode are shown. The wavelengths chosen are J, H, K, L, and M center wavelengths, and the fields are the central field, 2.4′, 4′, 6′, and 8′. The rms wavefront error is $\lesssim$25 % for all wavelengths and field angles as shown in the two upper plots. For the longer wavelengths, the wavefront error is actually $\lesssim$10 %, which is reasonably close to diffraction limit. These plots have to be regarded with some care though. The wavefront errors are calculated assuming perfect sampling with respect to diffraction limit for all wavelengths. We have those conditions barely at 5 μm. So the estimates at the lower wavelengths are very conservative. The spot diagram shows the spots at the detector from the central field to the edge field for all wavlelengths. Only for the very outer fields, the performance starts degrading. This is also visible in the enpixeled energy diagram at 5.0 μm. The absolute accuracy of the plot is limited due to sampling errors. But still the energy falling in one pixel (radius 13.5 μm) is reasonably close to the diffraction limited curve shown too. Again, for the edge field, the energy falling in one pixel is not as good, but acceptable, as about 70 % falls in two pixels, or 1″×1″,

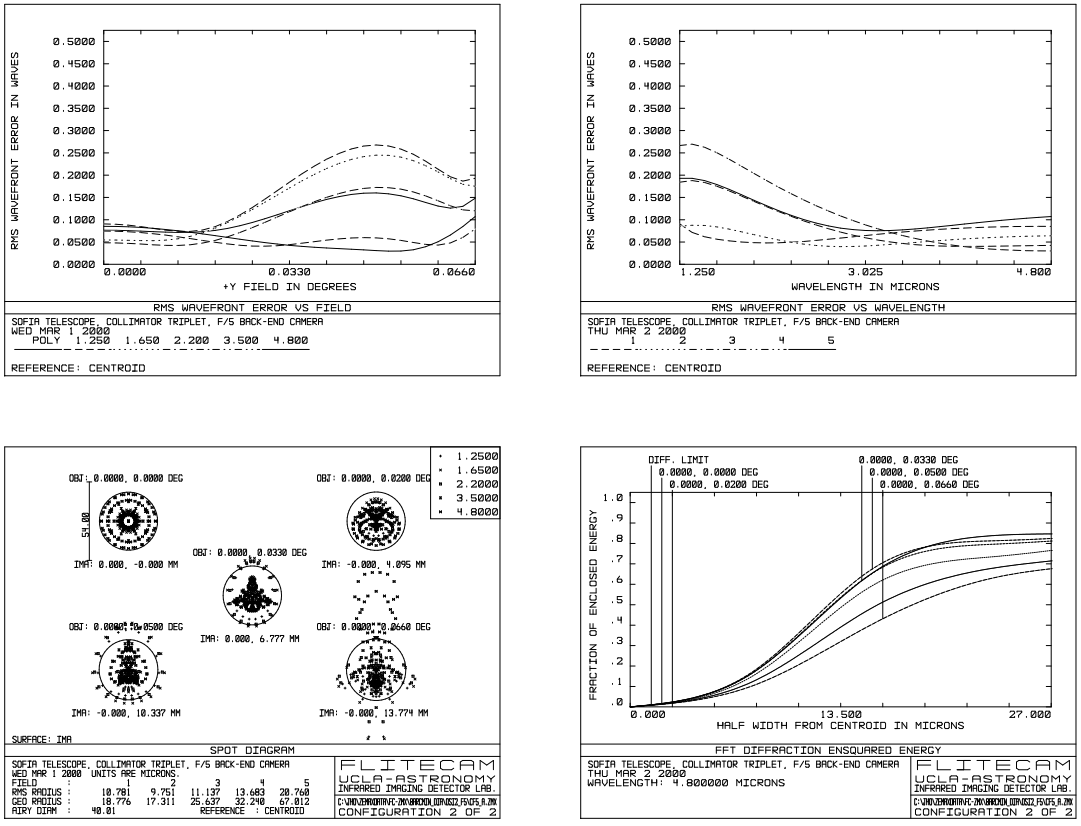

Figure 4. *Some sample performance plots for the imaging mode. The upper two plots show RMS wavefront error vs. field angle for various wavelengths (left) and vs. wavelength for various field angles (right), with field 1 being the center and field 5 the edge. The spot diagram is on the scale of 2 pixels and the airy disk at 3.5 μm is shown as a circle around the spot pattern (bottom left). The ensquared energy diagram is only shown for 5 μm (bottom right). See text for further details.*

which still accommodates the expected seeing on SOFIA, Lick and the Perkins. For the shorter wavelengths, the energy falling in one pixel is usually above 70 %, what is not presented here.

The predicted lateral color is less than one pixel across the wavelength range. The image distortion is about 2 % at the edge of the field compared to the central field, and splits by about 0.2 % or 1 pixel between 1 and 5 μm. Multi-color images should therefore not be affected by those aberrations. The chromatic aberration is well demonstrated to be low enough by the spot diagram of Fig. 4, which is plotted for all wavelengths. However, the direct evaluation of the chromatic aberration within Zemax gives a value of about 200 μm peak-to-valley over the entire wavelength range, which is close to what has been predicted, see Fig. 2.

3.2.3. The Pupil Viewing Lenses

The performance requirements on the pupil viewing mode are relatively loose, see Sect. 2. Still it was possible by means of a simple triplet, consisting of Silicon - BaF_2 - Silicon, to achieve very good performance results which are not sensitive to alignment variations or manufacturing tolerances, see Sect. 4. As shown in Fig. 3, there are three lenses which are being inserted into the optical path of the imaging mode. It has been optimized for 3.0 - 3.5 μm, yet it works very well from 3.0 - 4.0 μm. A summary of the performance results, similar to the one from the imaging mode is shown in Fig. 5, and the lens parameters are listed in Tab 3. Note that the enpixeled energy is polychromatic, reflecting the fact that the camera will be used with only an L - band filter in this mode. The filter, especially its thickness, is not yet fully specified. However, the effect of different filter thickness' can be compensated with the relative position of one or two of the pupil viewing lenses.

Lens #	Material	Radius front/back [mm]	Center Thickness [mm]	Diameter [mm]
1	Silicon	158.2420 (CC)/95.9866 (CX)	7.10	42
2	BaF_2	27.9908 (CC)/86.9442 (CX)	5.30	44
3	Silicon	83.9978 (CC)/59.7408 (CX)	6.92	54

Table 3. *The prescription data of the pupil viewing lenses. The first one sits in the second filter wheel, the other two are on a slide. Not listed are the air-spacings between the lenses, which are 2 mm or more. The high precision in the radii of curvature is a result of conversion from inches to millimeter. (CC = concave, CX = convex)*

3.3. Spectroscopy

FLITECAM will have a variable slit width of about 1″ to >4″ in order to accomodate for the expected worsening seeing from 5 μm to 1 μm. Assuming average conditions from 2.5 to 5.5 microns, the grisms for spectroscopy have been designed for a nominal slit width of 2″. As still a relatively high resolution of R≥1000 is desirable, the resolution is limited by the slit width rather than by diffraction. The fundamental equations that apply are[12]:

$$a\,(n - 1)\sin\Phi = m\lambda_c \quad (1)$$

$$R = \frac{f_{Coll}}{s}\,(n - 1)\tan\Phi, \quad (2)$$

with a the groove spacing, n the refractive index of the material, Φ the prism apex angle which is the same as the blaze angle, m the diffraction order, λ_c the center wavelength, that is not deviated in direction, R the resolution, f_{Coll} the focal length of the collimator, and s the slit width. Eq. (1) follows from applying Snell's law to the general grating equation. Eq. (2) has been expressed in a way that makes calculations easier for varying slit widths.

In order to achieve a resolution of about R = 1300 for a slit width of 2″ and a collimator focal length of $f_{Coll} = 550$ mm, we are planning to use either ZnSe or KRS-5 (both n≃2.4) direct ruled grisms with an apex angle of 40°. The grisms have to be direct ruled, as resin grisms have an absorption feature at around 3.4 μm originating from an organic C-H stretch in the epoxy.

Under the conditions of Nyquist sampling of the smallest resolution elements and filling the entire array, the filter bandwidths for two grisms, that also sort their orders are plotted in Fig. 6. In addition to the order sorting filters, also the standard filters planned for FLITECAM are shown, and one wide-band, SOFIA-specific KL-filter with a central obscuration as well. The detailed parameters of the two grisms are shown in Tab. 4. Each grism will be used

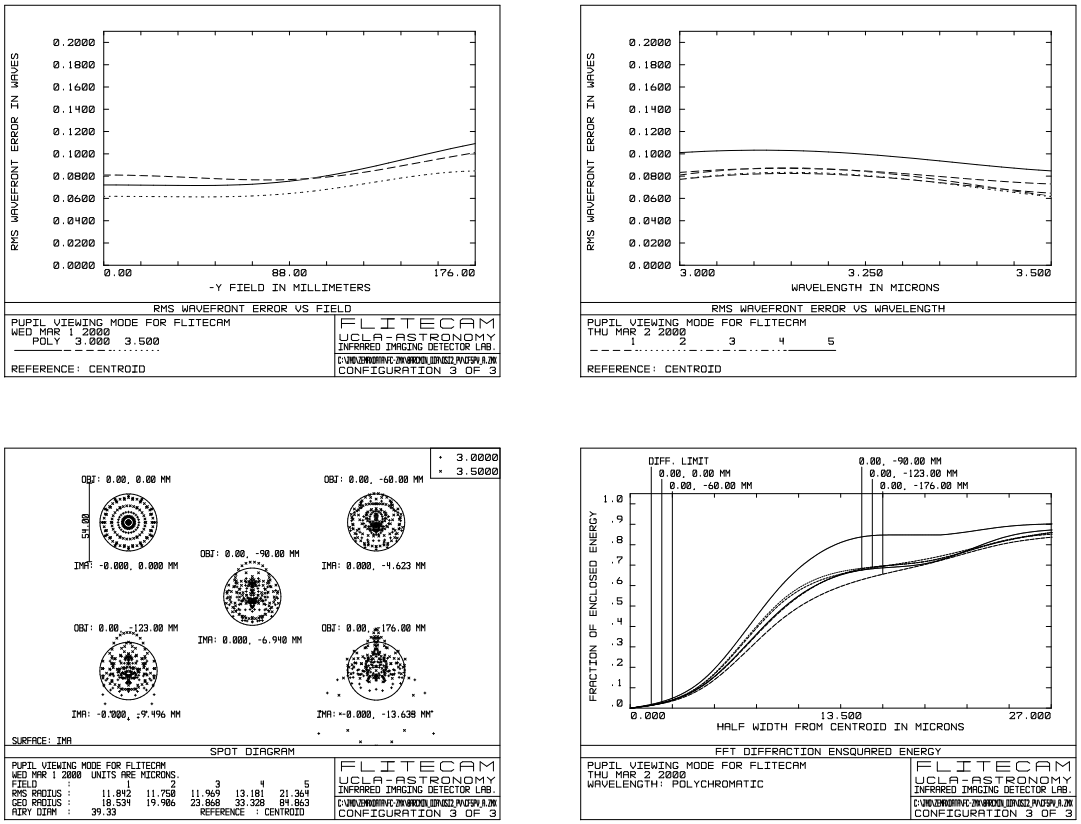

Figure 5. *Performance plots for the pupil viewing mode as in Fig. 4.*

Table 4. A Set of KRS-5/ZnSe Direct-Ruled Grisms for FLITECAM

Grism	Order	λ_c	Bandwidth	Resolution	Slit Width	Apex-$\measuredangle$	T=1/a
#1:	m=1	5.10 μm	4.61-5.58 μm	1790	1.5″	40°	176 lines/mm
	m=2	2.55 μm	2.30-2.80 μm	1330	2.0″		
	m=3	1.70 μm	1.53-1.86 μm	1330	2.0″		
				1790	1.5″		
	m=4	1.28 μm	1.16-1.40 μm	1330	2.0″		
#2:	m=2	4.75 μm	4.30-5.20 μm	1790	1.5″	40°	100 lines/mm
	m=3	3.17 μm	2.86-3.47 μm	1330	2.0″		
	m=4	2.38 μm	2.15-2.61 μm	1330	2.0″		
	m=5	1.90 μm	1.71-2.08 μm	1330	2.0″		

in multiple orders, but not all possible order sorting filters will be implemented for first light. We will focus on the wavelength regions, where no ground-based spectroscopy is possible. Anyway, while comparing the standard filters with the grism orders, one can see that the standard J- and H-filters can be used for the 3rd and 4th orders of grism # 1 and the M-filter falls entirely in the first order of grism # 2. Even for the higher orders, the grating efficiency should be above $\simeq$40 .[14]

4. TOLERANCE ANALYSIS

A detailed tolerance analysis has been done in order to estimate the performance that can be manufactured and aligned. In order to achieve as realistic estimates as possible, optics vendors[15] have been involved as well as pro-

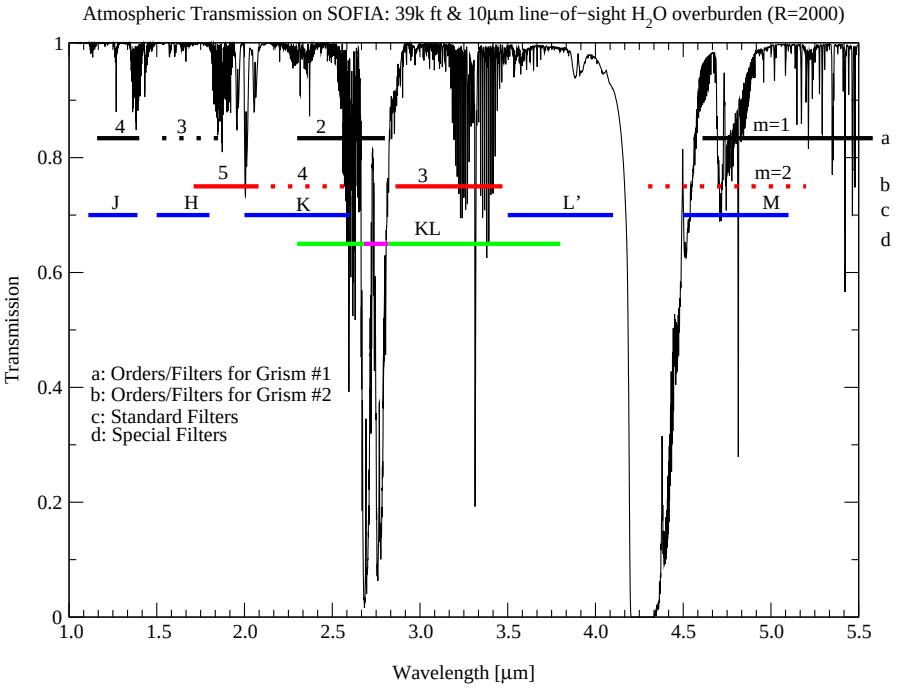

Figure 6. *Atmospheric transmission for a typical SOFIA altitude of 39,000 ft and a line-of-sight water vapor overburden of 10 μm for the FLITECAM wavelength range.*[13] *Overlayed are the spectroscopy filters, the standard filters and one special filter as planned so far. The dashed lines are grism orders, where no filter is being planned. Note that the KL filter will have an obscuration at the atmospheric CO_2 lines. Not shown are narrow-band imaging filters.*

fessional optics design consultants.[16] To do so, first certain allowable tolerances were specified in the design. The performance of a random set of optical designs, produced by means of a Monte-Carlo algorithm,[5] with manufacturing and alignment variations within those tolerances has then been monitored. This way, we were able to identify the most sensitive lens parameters, and whether or not those are possible to align and to fabricate.

The tolerances have been divided by lens group and by manufacturing tolerances and alignment tolerances. Manufacturing tolerances are the element center thickness (TTHI), the total indicator runout (TIR), surface irregularity (TIRR), and lens diameter (DIA). The design presented has testplate radii on every surface, so that tolerances on the radii of curvature could be neglected. The surface tilt, or wedge, and the decenter are covered by the total indicator runout and are therefore not mentioned seperately.
Alignment tolerances are basically lens element tilt (TET) and decenter (TED) and have to be accomplished by proper lens mounts.
Other than that, uncertainties in the index of refraction (TIND) have to be taken into account, as those are usually not perfectly known or measured at 77 K.

In Tab. 5 we give list of the tolerances that we found for our system. Not included are misalignments in the air-spacings. Those were typically identical to the element center thickness, so about $\pm 100\,\mu$m for the collimator spacings, and $\pm 50\,\mu$m else. This analysis is conservative in a sense, that it does not yet take into account that aligning certain parameters as e.g. the air-spacing between the optical elements can be used to compensate for manufacturing tolerances like element center thickness. This poses the requirement on the lens mount to make the air-spacers exchangeable. The optimum air-spacer can then be inserted once the lens has been fabricated and its center thickness been measured. Using the Monte-Carlo method mentioned above, we ran 40 sets of misalignments and vendor-fabrication tolerances, within the limits listed in Tab. 5, and checked the performance degradation. The performance parameters of a set with an average degradation are shown in Fig. 7. As one can see, most of the degradation starts at the outer 5 - 10 % of the field. This is clearly demonstrated by the ensquared energy diagram,

Lens	TTHI [μm]	TIR [μm]	TIRR [fringes @ 0.63 μm]	DIA [inch]	TET [μm]	TED [μm]	TIND
Collimator							
ZnS	± 100	$-0/+25$	2.5	$+0/-0.01$	± 100	± 100	± 0.0005
BaF_2	± 100	$-0/+25$	2.5	$+0/-0.01$	± 100	± 100	± 0.0005
LiF	± 100	$-0/+25$	2.5	$+0/-0.01$	± 100	± 100	± 0.0005
F/5 Imaging							
BaF_2	± 25	$-0/+25$	1.25	$+0/-0.005$	± 50	± 50	± 0.0005
ZnSe	± 50	$-0/+12.5$	1.25	$+0/-0.005$	± 50	± 50	± 0.0005
LiF	± 50	$-0/+25$	1.25	$+0/-0.005$	± 50	± 50	± 0.0005
ZnS	± 50	$-0/+25$	1.25	$+0/-0.005$	± 50	± 50	± 0.0005
ZnSe	± 50	$-0/+25$	1.25	$+0/-0.005$	± 50	± 50	± 0.0005
Pupil Viewing							
Silicon	± 100	$-0/+50$	1.25	$+0/-0.005$	± 100	± 100	± 0.001
BaF_2	± 100	$-0/+50$	1.25	$+0/-0.005$	± 100	± 100	± 0.0005
Silicon	± 100	$-0/+50$	1.25	$+0/-0.005$	± 100	± 100	± 0.001

Table 5. *Tolerances for the FLITECAM optics design. Abbreviations are explained in the text.*

where even at $6'$, the enpixeled energy still is close to diffraction limit, but at $8'$ is clearly worse. This can also be seen from the spot diagram of the outer field angle. We therefore feel, that we can achieve a reasonably good optics system within the allowed tolerances, that is not too far away from its nominal performance (compare with Fig. 4. Other Monte-Carlo systems, with an average or worse performance degradation have the same result; that the aberrations at the edge field are increasing faster than elsewhere. At the moment we are investigating ways to compensate for this with air-spacings, for example. A similar Monte-Carlo tolerance analysis for the pupil viewing mode has shown no significant aberrations that could fail the requirements.

Furthermore, all the lenses, except LiF, will be coated in order to achieve a good throughput. The coated lenses will have an average transmission of about 95 %. There is still a large potential of ghosts in the system from the reflected light from some of the 16 lens surfaces in the path in the imaging mode. However, a ghost analysis demonstrated that there is no ghost or pupil focus in the system.

ACKNOWLEDGMENTS

We would like to thank John Rayner for many helpful discussions on the infrared glasses used for FLITECAM and for providing the cryogenic refractive indices and thermal coefficients of expansion of the glasses used, E. W. Dunham for many helpful discussions during the project, R. E. Fischer from Optics-1 Inc. for reviewing the optics design, and Brad Picirillo for the support during the tolerance analysis.

REFERENCES

1. E. W. Dunham and J. Horn, "The SOFIA Test Plan: 0.3 - 5.0 μm," Tech. Rep. TN-EWD-010.R2, NASA Ames Research Center, Moffett Field, CA 94035-1000, 2000.
2. E. F. Erickson, "SOFIA: The next generation airborne observatory," *Space Sci. Reviews* **74**, pp. 91–100, 1995.
3. J. M. M. Horn, E. E. Becklin, G. Brims, J. Goulter, E. Kress, N. Magnone, I. S. McLean, J. Milburn, N. Molayem, H. Moseley, and M. Spencer, "FLITECAM - A near infrared camera for test and science applications on SOFIA," in *Optical and IR Telescope Instrumentation and Detectors*, *Proc. SPIE* **4014**, 2000.
4. D. F. Figer, I. S. McLean, and E. E. Becklin, "FLITECAM: a 1-5 μm camera for testing the performance of SOFIA," in *Infrared Astronomical Instrumentation*, A. Fowler, ed., *Proc. SPIE* **3354**, pp. 1179–1184, 1998.
5. Focus Software Inc., P. O. Box 18228, Tucson, AZ, 85731.
6. W. J. Smith, *Modern Optical Engineering*, Optical and Electro-Optical Engineering Series, McGraw Hill, first ed., 1990.

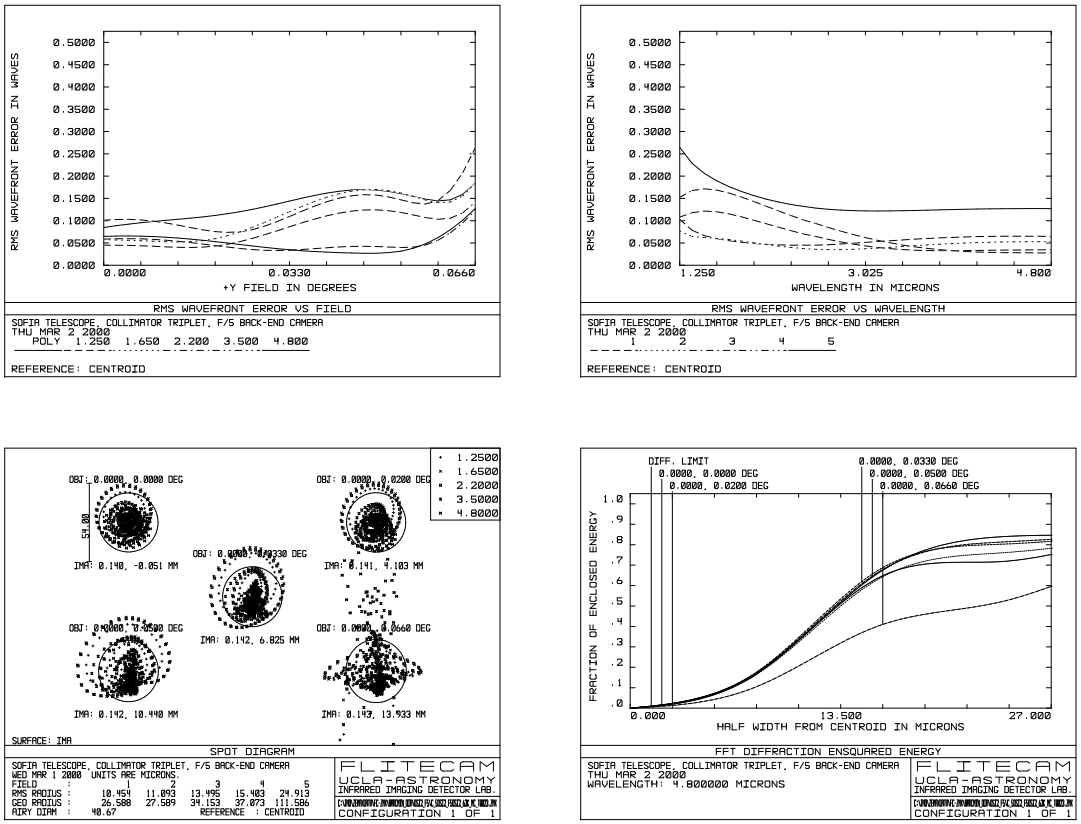

Figure 7. *RMS wavefront errors, spot diagram and ensquared energy diagram for a Monte-Carlo design. This design presents an average performing set out of 40 random sets of tolerances and mis-alignments as listed in Tab. 5. These plots have to be compared with the ones of Fig. 4, showing the nominal performance of the design. See caption of Fig. 4 for an explanation of the plots and text for discussion.*

7. W. J. Smith, *Modern Lens Design*, Optical and Electro-Optical Engineering Series, McGraw Hill, second ed., 1992.
8. J. T. Rayner, priv. comm., 1999.
9. H. Epps, priv. comm., 1999.
10. J. T. Rayner, D. W. Toomey, P. M. Onaka, A. J. Denault, W. E. Stahlberger, D. Y. Watanabe, and S. Wang, "SpeX: a medium-resolution IR spectrograph for IRTF," in *Infrared Astronomical Instrumentation*, A. Fowler, ed., *Proc. SPIE* **3354**, pp. 468–479, 1998.
11. R. Kingslake, *Lens Design Fundamentals*, Academic Press, 1978.
12. I. S. Mclean, *Electronic Imaging in Astronomy*, Wiley, 1997.
13. S. D. Lord, "A New Software Tool for Computing Earth's Atmospheric Transmission of Near- and Far-Infrared Radiation," NASA Technical Memorandum 103957, NASA Ames Research Center, Moffett Field, CA 94035-1000, 1992.
14. J. T. Rayner, "Evaluation of a solid KRS-5 grism for infrared astronomy," in *Infrared Astronomical Instrumentation*, A. Fowler, ed., *Proc. SPIE* **3354**, pp. 289–294, 1998.
15. B. Picirillo, Optical Solutions Inc., priv. comm., 2000.
16. R. E. Fischer, Optics 1 Inc., priv. comm., 2000.